Since January 2020 Elsevier has created a COVID-19 resource centre with free information in English and Mandarin on the novel coronavirus COVID-19. The COVID-19 resource centre is hosted on Elsevier Connect, the company's public news and information website.

Biologicals 75 (2022) 29–36

Contents lists available at ScienceDirect

Biologicals

journal homepage: www.elsevier.com/locate/biologicals

Emerging genetic diversity of SARS-CoV-2 RNA dependent RNA polymerase (RdRp) alters its B-cell epitopes

Sushant Kumar [b], Khushboo Kumari [b], Gajendra Kumar Azad [b,*]

[b] Department of Zoology, Patna University, Patna, 800005, Bihar, India

ARTICLE INFO

Keywords:
COVID-19
SARS-CoV-2
Mutations
B cell epitopes
RNA dependent RNA polymerase (RdRp)
India

ABSTRACT

The RNA dependent RNA polymerase (RdRp) plays crucial role in virus life cycle by replicating the viral genome. The SARS-CoV-2 is an RNA virus that rapidly spread worldwide and acquired mutations. This study was carried out to identify mutations in RdRp as the SARS-CoV-2 spread in India. We compared 50217 RdRp sequences reported from India with the first reported RdRp sequence from Wuhan, China to identify 223 mutations acquired among Indian isolates. Our protein modelling study revealed that several mutants can potentially alter stability and flexibility of RdRp. We predicted the potential B cell epitopes contributed by RdRp and identified thirty-six linear continuous and twenty-five discontinuous epitopes. Among 223 RdRp mutants, 44% of them localises in the B cell epitopes region. Altogether, this study highlights the need to identify and characterize the variations in RdRp to understand the impact of these mutations on SARS-CoV-2.

1. Introduction

SARS-CoV-2 genome encodes 29 protein molecules which are categorised into three groups including structural, non-structural and accessory proteins. SARS-CoV-2 has four structural proteins namely Spike glycoprotein, Membrane protein, Envelope protein and Nucleocapsid Phosphoprotein [1]. It also encodes sixteen non-structural proteins (Nsp1-16) and nine accessory proteins. The 16 non-structural proteins are synthesised as a single polypeptide molecule of 7096 amino acids known as Orf1ab that is subsequently cleaved into 16 separate proteins [2]. The RNA dependent RNA polymerase (RdRp), also known as Nsp12, is a non-structural protein that replicates SARS-CoV-2 RNA genome [1]. It associates with Nsp7 and Nsp8 and exist as a trimeric complex inside the viral envelope structure [3]. By itself, RdRp has a very weak polymerase activity; however, the complex of RdRp with Nsp7 and Nsp8 significantly increases RdRp processivity and template affinity [4].

RdRp of SARS-CoV-2 is 932 residues in length and contains distinct polymerase and nucleotide binding domains with a central connecting domain. Structurally, RdRp is comprised of an N-terminal β-hairpin (residues 31–50) followed by an extended nidovirus RdRp-associated nucleotidyl-transferase domain (NiRAN, residues 115–250) [5]. Following the NiRAN domain is an interface domain (residues 251–365) connected to the RdRp domain (residues 366–920). Further, the domains of RdRp arranges in such a way that it forms a canonical right-handed cup configuration [6], with the finger subdomain (resides 397–581 and residues 621–679) forming a closed circle with the thumb subdomain (residues 819–920) [5].

Bioinformatics has enabled researchers to study large number of epitopes and their properties without the risk of growing pathogens. It has drastically reduced the cost of study and faster output over the conventional methods of vaccine study. Further, the amalgamation of various genome-wide studies with the immunoinformatics has revolutionised the identification of epitopes contributed by a protein or virus and accelerated our understanding of vaccine design and action [7,8]. Several studies show that SARS-CoV-2 RdRp participates in host immune response and thus provides insights into viral pathogenesis [9–12]. RdRp stimulates a considerable amount of immunogenicity due to its lower glycosylation density as compared to other structural proteins and several studies have revealed that RdRp induces both innate and adaptive immune response of host [9–11]. Another study has revealed that RdRp, suppresses host antiviral responses by inhibiting IRF3 nuclear translocation [12]. Furthermore, RdRp is one of the most conserved enzyme across several viral species, such as influenza virus, hepatitis C virus (HCV), ZIKA virus (ZIKV), and coronavirus (CoV), suggesting that its function and mechanism of action might be well conserved [13,14]. As the SARS-CoV-2 spread to new geographical areas, it started to mutate [14]. The mutations acquired by the SARS-CoV-2 are retained as

* Corresponding author.
E-mail address: gkazad@patnauniversity.ac.in (G.K. Azad).

https://doi.org/10.1016/j.biologicals.2021.11.002
Received 8 May 2021; Received in revised form 10 October 2021; Accepted 12 November 2021
Available online 17 November 2021

a consequence of natural selection, if the variants are more adaptable. In order to understand the variations occurring in RdRp among Indian geographical area, we analysed 50217 RdRp sequences reported from India to identified 223 mutations. The B cell epitopes contributed by RdRp were predicted in silico and the mutations were also mapped.

2. Material and methods

2.1. Protein sequences retrieval and analysis

The sequences used in this study are available on publicly accessible CoVal database (https://coval.ccpem.ac.uk/). A total of 50217 SARS-CoV-2 sequences reported between Jan 2020 till Sept 2021 from different geographical locations within India were used in this study. The mutations occurring in SARS-CoV-2 were obtained from CoVal webserver. The CoVal Webserver uses sequences from the GISAID repository and updates its information at frequent intervals.

2.2. Identification of RdRp mutants by multiple sequence alignments (MSAs)

In order to identify the variations present in the RdRp sequences among Indian isolates of SARS-CoV-2, the MSAs were conducted by Clustal omega programe [15] as described earlier [16].

2.3. B cell epitope prediction

The prediction of linear continuous B cell epitopes were conducted by IEDB [17]. The IEDB webserver provides training set for evaluation of existing epitope prediction methods and constitute platform for development of novel and better algorithm for prediction. IEDB webserver also provides tools for the prediction of linear B-cell epitopes from protein sequence including amino acid scales and HMMs, DiscoTope, ElliPro, Paratome, and PIGS. The IEDB contains epitopes derived from the peer-reviewed literature, patent applications, direct submission, and other publicly available databases, for example, FIMM, HLA Ligand database, and MHC binding database. The IEDB prediction method known as 'Bepipred linear epitope prediction method 2.0' was used in this study. For this prediction the threshold value of 0.500 was used during the evaluation. The prediction of discontinuous B cell epitopes was performed by an online tool 'DiscoTope 2.0'. For this prediction the threshold value was set at −3.7.

2.4. Protein modelling studies

We performed protein modelling studies by DynaMut programe [18] as described earlier [19]. The DynaMut web server was used for analysing thermodynamic stability of different RdRp mutations observed in this study. The DynaMut webserver introduces dynamics component for mutational analysis to predict difference in free energy (ΔΔG) and vibrational entropy (ΔΔS). This webserver implements Normal mode analysis (NMA) through two different approaches, Bio3D and ENCoM, that provide rapid and simplified access to analyse protein dynamics and stability resulting from vibrational entropy changes [18]. It also enables to assess the effects of missense mutations on protein stability and provide comprehensive suite for protein motion and flexibility analysis and visualization (http://biosig.unimelb.edu.au/dynamut/). For this study, we used recently reported structure of RdRp (PDB ID: 7BV1) [5]. The effect of mutations on protein is shown in terms of difference in free energy (ΔΔG). DynaMut provides difference in vibrational entropy (ΔΔSvib ENCOM) between the wild type and mutant protein. We ran DynaMut webserver to calculate the ΔΔG and ΔΔSvib ENCOM that provides the impact of mutation on protein structure and stability.

3. Results

3.1. RdRp is frequently mutated among Indian isolates of SARS-CoV-2

In order to identify the mutations in RdRp, we used CoVal webserver that compares the first reported sequence of RdRp from Wuhan, China with the sequences reported from India. Till Sept 2021, a total of 50217 sequences has been analysed by CoVal webserver. The data revealed 223 mutations present among the Indian sequences of RdRp as shown in Table 1. The mutations are also demonstrated on the schematic representation of RdRp as shown in Fig. 1A. Our result show that the mutations are spreading all over the RdRp polypeptide sequence. The distribution of mutations in different domains of RdRp has been highlighted in Fig. 1A. This data strongly indicates that RdRp is one of the most frequently mutated proteins of SARS-CoV-2 because we observed 223 mutations till Sept 2021. Furthermore, we looked at the time course of the samples used for mutational study by CoVal webserver. This webserver shows the monthly appearance of new mutations from India. Based on the mutational analysis of RdRp by CoVAL webserver, we observe that during initial phase of COVID19 pandemic, the rate of occurrence of new mutations were high but it slowed down as the time progresses (Fig. 1B), suggesting that the virus is attaining mutational stability over time.

3.2. Mutations affect RdRp protein dynamic stability and flexibility

We performed protein modelling studies using DynaMut programe to understand, if the mutation observed in RdRp can alter protein structural integrity. Our data revealed that mutations at 89 positions cause stabilisation in protein structure (positive ΔΔG) as shown in Table 1, maximum positive ΔΔG was obtained for Q822K (1.801 kcal/mol). Similarly, the mutations at 111 positions cause destabilisation (negative ΔΔG) in protein structure upon mutation (Table 1), maximum negative ΔΔG was obtained for the mutant I244T (-2.233 kcal/mol).

Subsequently, we measured the changes in vibrational entropy energy (ΔΔSVibENCoM) between the wild type and the mutant. Our data revealed that mutation at 89 positions causes increase in flexibility of mutant protein (positive ΔΔSVibENCoM). The maximum positive ΔΔSVibENCoM was obtained for T929I (4.55 kcal.mol-1.K-1) mutant. Similarly, the mutations at rest of the 111 positions cause rigidification of protein structure (negative ΔΔSVibENCoM) in protein structure upon mutation (Table 1). The maximum negative ΔΔSVibENCoM was obtained for Q932H (-4.93 kcal.mol-1.K-1) mutant. Altogether, our data revealed that the mutation observed in RdRp affects both protein dynamicity and flexibility.

3.3. Identification of B cell epitopes of RdRp

The continuous B-cell epitopes of RdRp were predicted by IEDB webserver tool and the epitopes are shown in Fig. 2A. The yellow area of the graph corresponds to those regions of the RdRp that can potentially contribute to the B cell epitopes. Our data demonstrated thirty-six epitopes of varying lengths that could potentially act as B cell epitopes (Fig. 2B). Among those peptides, the 'peptide 18' is the largest epitope of 44 amino acids (from RdRp residue 482 to 525). Similarly, peptide 5, 19, 30, 31 and 34 are comprised of single amino acid only (Fig. 2B).

Subsequently, we predicted the B cell epitopes of RdRp based on its three dimensional structure using DiscoTope 2.0 webserver tool [20]. Our analysis revealed twenty-five discontinuous epitopes of RdRp having high score. The locations of these epitopes are listed in Fig. 2C along with its propensity and DiscoTope score. Among discontinuous epitopes, approximately 80% of them (20 out of 25) reside towards the C-terminal end of RdRp (from residue 800 to 932) as shown in Fig. 2C. Altogether, our data revealed B cell epitopes contributed by RdRp.

Table 1
The list demonstrates the location and details of mutations of RdRp identified by CoVal webserver. The RdRp sequence reported from Wuhan, China was used as wild type sequence for this analysis. The 50217 sequences of RdRp reported from India (till Sept 2021) were used for identifying mutations and their frequency. The ΔΔG and ΔΔSvib ENCOM values were obtained by protein modelling using DynaMut programe. The positive and negative ΔΔG represents increase and decrease in protein stability upon mutation. Similarly, the positive and negative ΔΔSvib ENCOM represents the increase in flexibility and rigidity upon mutations. The mutation that localises in the unmodeled region of RdRp was not used in the analysis of ΔΔG and ΔΔSvib ENCOM and they were left blank (denotes by -) in table. P stands for Polar, NP stands for Non-Polar.

Serial Number	Nsp12 mutations	Polarity changes	Charge changes	Frequency of mutation	ΔΔG (kcal/mol)	ΔΔSVib ENCoM (kcal.mol-1.K-1)
1	A2V	NP to NP	Neutral to Neutral	3	–	–
2	S6L	P to NP	Neutral to Neutral	12	–	–
3	C12R	P to P	Neutral to Basic	2	–	–
4	A16V	NP to NP	Neutral to Neutral	8	–	–
5	A16E	NP to P	Neutral to Acidic	2	–	–
6	T20A	P to NP	Neutral to Neutral	11	–	–
7	G25D	NP to P	Neutral to Acidic	4	–	–
8	T26I	P to NP	Neutral to Neutral	13	–	–
9	Y32H	P to P	Neutral to Basic	2	−0.349	0.090
10	D40A	P to NP	Acidic to Neutral	4	−0.139	0.021
11	V42L	NP to NP	Neutral to Neutral	2	0.347	−0.342
12	G44V	NP to NP	Neutral to Neutral	2	−1.011	−0.103
13	A46T	NP to P	Neutral to Neutral	2	−1.031	−0.174
14	K59 N	P to P	Basic to Neutral	12	–	–
15	D62Y	P to P	Acidic to Neutral	3	–	–
16	N64D	P to P	Neutral to Acidic	2	–	–
17	D67 N	P to P	Acidic to Neutral	4	–	–
18	T85I	P to NP	Neutral to Neutral	14	−0.707	−0.074
19	K91R	P to P	Basic to Basic	11	−0.143	−0.066
20	K91E	P to P	Basic to Acidic	2	−0.187	0.416
21	K91 N	P to P	Basic to Neutral	2	−0.311	0.295
22	P94L	NP to NP	Neutral to Neutral	6	0.858	−0.242
23	P94S	NP to P	Neutral to Neutral	3	−0.035	−0.131
24	A95S	NP to P	Neutral to Neutral	5	−1.317	−0.172
25	A95V	NP to NP	Neutral to Neutral	4	−0.669	−0.627
26	A97V	NP to NP	Neutral to Neutral	438	0.469	−1.020
27	G108V	NP to NP	Neutral to Neutral	8	–	–
28	D109G	P to NP	Acidic to Neutral	3	–	–
29	D109Y	P to P	Acidic to Neutral	2	–	–
30	R118C	P to P	Basic to Neutral	4	0.005	0.055
31	M124I	NP to NP	Neutral to Neutral	6	−0.088	0.250
32	V128I	NP to NP	Neutral to Neutral	5	1.237	−0.268
33	G137S	NP to P	Neutral to Neutral	2	−1.389	0.029
34	C139S	P to P	Neutral to Neutral	2	−0.460	−0.227
35	D140Y	P to P	Acidic to Neutral	6	−0.105	0.035
36	D140G	P to NP	Acidic to Neutral	3	−0.180	0.035
37	T141I	P to NP	Neutral to Neutral	11	1.041	−0.231
38	I145V	NP to NP	Neutral to Neutral	4	−0.190	0.408
39	D153Y	P to P	Acidic to Neutral	10	0.961	0.049
40	D154G	P to NP	Acidic to Neutral	2	−0.771	0.111
41	K160 N	P to P	Basic to Neutral	6	−0.089	−0.029
42	D161Y	P to P	Acidic to Neutral	2	1.107	−0.621
43	W162C	NP to P	Neutral to Neutral	3	−1.169	1.004
44	P169S	NP to P	Neutral to Neutral	3	0.478	−0.232
45	D170G	P to NP	Acidic to Neutral	3	−0.527	0.156
46	D170Y	P to P	Acidic to Neutral	3	−0.089	0.154
47	R173S	P to P	Basic to Neutral	4	−0.412	0.203
48	R173C	P to P	Basic to Neutral	2	−0.283	0.168
49	R173H	P to P	Basic (strongly) to Basic (weakly)	2	−0.284	0.010
50	A176T	NP to P	Neutral to Neutral	2	0.032	−0.721
51	A185V	NP to NP	Neutral to Neutral	11	−0.179	−0.369
52	A185S	NP to P	Neutral to Neutral	2	–	–
53	A195D	NP to P	Neutral to Acidic	2	−0.478	−0.397
54	M196I	NP to NP	Neutral to Neutral	7	−0.554	0.094
55	R197Q	P to P	Basic to Neutral	3	−0.483	0.096
56	R197L	P to NP	Basic to Neutral	2	−0.109	0.109
57	I223 M	NP to NP	Neutral to Neutral	13	−0.051	−0.084
58	T225I	P to NP	Neutral to Neutral	2	0.090	−0.076
59	P227L	NP to NP	Neutral to Neutral	245	0.360	−0.332
60	P227T	NP to P	Neutral to Neutral	2	0.459	−0.375
61	G228S	NP to P	Neutral to Neutral	18	−1.113	−0.158
62	V231I	NP to NP	Neutral to Neutral	3	−0.529	0.229
63	I244T	NP to P	Neutral to Neutral	85	−3.236	0.746
64	T248I	P to NP	Neutral to Neutral	7	0.452	−0.080
65	R249S	P to P	Basic to Neutral	7	−0.672	0.320
66	R249G	P to NP	Basic to Neutral	2	−0.382	0.504
67	R249 M	P to NP	Basic to Neutral	2	0.825	−0.111
68	A250V	NP to NP	Neutral to Neutral	5	−0.237	−0.482

(*continued on next page*)

Table 1 (*continued*)

Serial Number	Nsp12 mutations	Polarity changes	Charge changes	Frequency of mutation	ΔΔG (kcal/mol)	ΔΔSVib ENCoM (kcal.mol-1.K-1)
69	T252I	P to NP	Neutral to Neutral	4	0.265	−0.060
70	A253V	NP to NP	Neutral to Neutral	2	−0.415	−0.586
71	E254D	P to P	Acidic to Acidic	2	−1.136	0.395
72	H256Y	P to P	Basic to Neutral	3	−0.411	−0.074
73	V257F	NP to NP	Neutral to Neutral	5	−0.485	0.162
74	K263 N	P to P	Basic to Neutral	5	−0.336	0.316
75	P264S	NP to P	Neutral to Neutral	4	−0.715	0.098
76	D269 N	P to P	Acidic to Neutral	34	−0.258	0.080
77	L270F	NP to NP	Neutral to Neutral	3	0.390	−0.209
78	E278D	P to P	Acidic to Acidic	3	−0.714	0.103
79	R279S	P to P	Basic to Neutral	3	−2.849	1.063
80	L282I	NP to NP	Neutral to Neutral	3	−0.287	0.096
81	D284Y	P to P	Acidic to Neutral	7	0.346	−0.459
82	Q292H	P to P	Neutral to Basic	2	0.171	0.070
83	T293I	P to NP	Neutral to Neutral	5	0.264	−0.016
84	V299F	NP to NP	Neutral to Neutral	4	0.240	−0.143
85	L302F	NP to NP	Neutral to Neutral	3	−0.363	0.045
86	A311S	NP to P	Neutral to Neutral	8	−0.229	−0.014
87	V315A	NP to NP	Neutral to Neutral	3	−1.724	0.711
88	F317L	NP to NP	Neutral to Neutral	2	0.045	0.379
89	T319I	P to NP	Neutral to Neutral	35	1.052	−0.244
90	P323L	NP to NP	Neutral to Neutral	11094	0.530	−0.252
91	P323F	NP to NP	Neutral to Neutral	24	0.297	−0.199
92	P323V	NP to NP	Neutral to Neutral	3	0.578	−0.313
93	S325I	P to NP	Neutral to Neutral	2	1.763	−0.574
94	P328S	NP to P	Neutral to Neutral	2	−0.425	0.065
95	L329I	NP to NP	Neutral to Neutral	15	0.081	0.231
96	V330A	NP to NP	Neutral to Neutral	38	–	–
97	V330L	NP to NP	Neutral to Neutral	5	0.025	−0.103
98	G337C	NP to P	Neutral to Neutral	2	−1.187	0.219
99	Y346H	P to P	Neutral to Basic	2	−0.021	0.619
100	V354L	NP to NP	Neutral to Neutral	21	−0.162	−0.387
101	V354A	NP to NP	Neutral to Neutral	4	−1.811	0.277
102	Q357H	P to P	Neutral to Basic	7	1.218	−0.094
103	D358G	P to NP	Acidic to Neutral	3	−0.096	0.357
104	A379V	NP to NP	Neutral to Neutral	7	0.624	−0.529
105	A379S	NP to P	Neutral to Neutral	2	1.586	−0.510
106	M380I	NP to NP	Neutral to Neutral	6	−0.487	0.551
107	A382V	NP to NP	Neutral to Neutral	3	0.596	−0.438
108	A383S	NP to P	Neutral to Neutral	2	−0.131	−0.021
109	T394 M	P to NP	Neutral to Neutral	3	0.947	−0.648
110	A400S	NP to P	Neutral to Neutral	52	0.437	−0.127
111	T402I	P to NP	Neutral to Neutral	6	0.301	0.039
112	V405F	NP to NP	Neutral to Neutral	3	0.955	−0.639
113	A406S	NP to P	Neutral to Neutral	7	0.497	−0.246
114	A406V	NP to NP	Neutral to Neutral	2	−0.148	−0.047
115	D418E	P to P	Acidic to Acidic	2	0.915	−0.258
116	A423V	NP to NP	Neutral to Neutral	12	0.732	−0.338
117	S434Y	P to P	Neutral to Neutral	2	0.277	−0.606
118	V435I	NP to NP	Neutral to Neutral	4	0.150	−0.391
119	V435F	NP to NP	Neutral to Neutral	2	−0.063	−1.096
120	A443V	NP to NP	Neutral to Neutral	4	0.937	−0.250
121	A443S	NP to P	Neutral to Neutral	2	−0.013	−0.135
122	Q444H	P to P	Neutral to Basic	5	1.310	−0.346
123	A449V	NP to NP	Neutral to Neutral	7	0.871	−0.560
124	A449S	NP to P	Neutral to Neutral	2	−0.265	0.016
125	I450V	NP to NP	Neutral to Neutral	2	−1.121	0.580
126	Y458H	P to P	Neutral to Basic	3	−0.169	0.293
127	P461S	NP to P	Neutral to Neutral	8	−0.475	0.055
128	M463I	NP to NP	Neutral to Neutral	19	0.483	0.250
129	C464F	P to NP	Neutral to Neutral	2	1.251	−1.092
130	I466T	NP to P	Neutral to Neutral	2	−2.428	0.355
131	V473F	NP to NP	Neutral to Neutral	24	−0.802	−0.941
132	V476A	NP to NP	Neutral to Neutral	3	−0.477	0.578
133	K478 N	P to P	Basic to Neutral	60	−1.105	0.533
134	I494V	NP to NP	Neutral to Neutral	2	−0.044	0.027
135	L514F	NP to NP	Neutral to Neutral	2	−0.300	−0.066
136	Y521H	P to P	Neutral to Basic	4	−0.048	0.764
137	A526V	NP to NP	Neutral to Neutral	4	0.305	−0.109
138	A526S	NP to P	Neutral to Neutral	3	−0.315	−0.121
139	A529V	NP to NP	Neutral to Neutral	16	−0.273	−0.068
140	A529T	NP to P	Neutral to Neutral	3	−0.874	0.002
141	A529S	NP to P	Neutral to Neutral	2	−0.884	−0.059
142	I536T	NP to P	Neutral to Neutral	3	–	–
143	L544I	NP to NP	Neutral to Neutral	7	0.224	0.060

(*continued on next page*)

Table 1 (*continued*)

Serial Number	Nsp12 mutations	Polarity changes	Charge changes	Frequency of mutation	ΔΔG (kcal/mol)	ΔΔSVib ENCoM (kcal.mol-1.K-1)
144	A544V	NP to NP	Neutral to Neutral	2	0.325	−0.547
145	I562V	NP to NP	Neutral to Neutral	2	−0.801	0.215
146	I579V	NP to NP	Neutral to Neutral	3	−0.573	0.414
147	T586P	P to NP	Neutral to Neutral	2	−0.213	0.662
148	V588L	NP to NP	Neutral to Neutral	4	0.599	−0.117
149	T591I	P to NP	Neutral to Neutral	4	1.218	−0.416
150	M601I	NP to NP	Neutral to Neutral	18	−0.362	−0.033
151	V605A	NP to NP	Neutral to Neutral	18	−1.528	0.596
152	H613Y	P to P	Basic to Neutral	20	0.836	−0.213
153	M629I	NP to NP	Neutral to Neutral	6	−0.428	0.170
154	L636F	NP to NP	Neutral to Neutral	4	−0.115	−0.435
155	L636I	NP to NP	Neutral to Neutral	2	0.569	0.041
156	L638F	NP to NP	Neutral to Neutral	6	−0.167	−0.297
157	T643I	P to NP	Neutral to Neutral	10	−0.383	−0.074
158	T644 M	P to NP	Neutral to Neutral	3	−0.084	−0.037
159	S647I	P to NP	Neutral to Neutral	29	−0.272	0.166
160	S649L	P to NP	Neutral to Neutral	2	0.684	−0.422
161	A656S	NP to P	Neutral to Neutral	20	−1.416	0.063
162	M666I	NP to NP	Neutral to Neutral	6	−0.229	0.365
163	M668I	NP to NP	Neutral to Neutral	11	0.104	0.066
164	G671S	NP to P	Neutral to Neutral	2665	0.786	−0.246
165	G671A	NP to NP	Neutral to Neutral	2	1.315	−0.906
166	V675I	NP to NP	Neutral to Neutral	49	0.050	−0.115
167	C697F	P to NP	Neutral to Neutral	3	−1.055	−0.979
168	A699S	NP to P	Neutral to Neutral	4	−2.233	−0.185
169	T710 N	P to P	Neutral to Neutral	2	0.703	−0.185
170	A716T	NP to P	Neutral to Neutral	2	0.285	−0.035
171	K718 N	P to P	Basic to Neutral	5	−0.208	0.051
172	H725Y	P to P	Basic to Neutral	6	0.240	0.166
173	E729K	P to P	Acidic to Basic	2	0.825	−0.139
174	N734D	P to P	Neutral to Acidic	4	−0.338	0.227
175	D736 N	P to P	Acidic to Neutral	3	0.006	−0.049
176	D738Y	P to P	Acidic to Neutral	5	0.861	−0.137
177	T739I	P to NP	Neutral to Neutral	4	0.272	0.008
178	E744D	P to P	Acidic to Acidic	11	−0.566	0.229
179	M756I	NP to NP	Neutral to Neutral	11	1.019	0.205
180	S768 N	P to P	Neutral to Neutral	2	−0.152	−0.012
181	G774C	NP to P	Neutral to Neutral	4	0.107	−0.086
182	L775P	NP to NP	Neutral to Neutral	2	−0.600	0.754
183	V776L	NP to NP	Neutral to Neutral	3	−0.017	−0.160
184	S778C	P to P	Neutral to Neutral	3	0.409	−0.305
185	S778 N	P to P	Neutral to Neutral	2	0.687	−0.195
186	K780R	P to P	Basic to Basic	5	1.115	−0.590
187	E796D	P to P	Acidic to Acidic	4	−0.269	0.244
188	T801I	P to NP	Neutral to Neutral	5	0.114	−0.047
189	L803I	NP to NP	Neutral to Neutral	2	0.397	−0.105
190	L805I	NP to NP	Neutral to Neutral	3	−0.189	0.217
191	T806I	P to NP	Neutral to Neutral	29	0.151	−0.065
192	P809R	NP to P	Neutral to Basic	5	−0.615	−0.234
193	M818I	NP to NP	Neutral to Neutral	2	0.129	0.221
194	Q822H	P to P	Neutral to Basic	60	0.006	0.514
195	Q822K	P to P	Neutral to Basic	2	1.801	−0.467
196	G823C	NP to P	Neutral to Neutral	4	0.442	−0.644
197	G823D	NP to P	Neutral to Acidic	2	0.467	−0.400
198	D824Y	P to P	Acidic to Neutral	6	−0.451	0.111
199	V827L	NP to NP	Neutral to Neutral	3	0.471	−0.340
200	L829F	NP to NP	Neutral to Neutral	4	−1.408	0.045
201	P834L	NP to NP	Neutral to Neutral	3	1.266	−0.943
202	V848L	NP to NP	Neutral to Neutral	12	0.194	−0.201
203	V848I	NP to NP	Neutral to Neutral	2	−0.732	0.119
204	M855I	NP to NP	Neutral to Neutral	6	−0.312	0.223
205	I856V	NP to NP	Neutral to Neutral	2	−0.635	0.307
206	T870I	P to NP	Neutral to Neutral	10	0.654	−0.440
207	P873S	NP to P	Neutral to Neutral	6	−0.054	0.023
208	E876D	P to P	Acidic to Acidic	2	−1.338	1.031
209	A878S	NP to P	Neutral to Neutral	2	1.053	−0.488
210	D879Y	P to P	Acidic to Neutral	6	1.218	−0.559
211	V880I	NP to NP	Neutral to Neutral	34	−0.087	−0.146
212	D893Y	P to P	Acidic to Neutral	7	0.088	−0.168
213	T896I	P to NP	Neutral to Neutral	2	–	–
214	M899I	NP to NP	Neutral to Neutral	4	–	–
215	V905I	NP to NP	Neutral to Neutral	38	–	–
216	M906I	NP to NP	Neutral to Neutral	2	–	–
217	T908I	P to NP	Neutral to Neutral	5	–	–
218	S913L	P to NP	Neutral to Neutral	19	−0.116	0.012

(*continued on next page*)

Table 1 (*continued*)

Serial Number	Nsp12 mutations	Polarity changes	Charge changes	Frequency of mutation	ΔΔG (kcal/mol)	ΔΔSVib ENCoM (kcal.mol-1.K-1)
219	R914K	P to P	Basic to Basic	9	−0.240	0.168
220	P918L	NP to NP	Neutral to Neutral	4	0.199	−0.711
221	E922D	P to P	Acidic to Acidic	8	−1.106	0.193
222	T929I	P to NP	Neutral to Neutral	2	0.075	4.551
223	Q932H	P to P	Neutral to Basic	2	1.077	−4.934

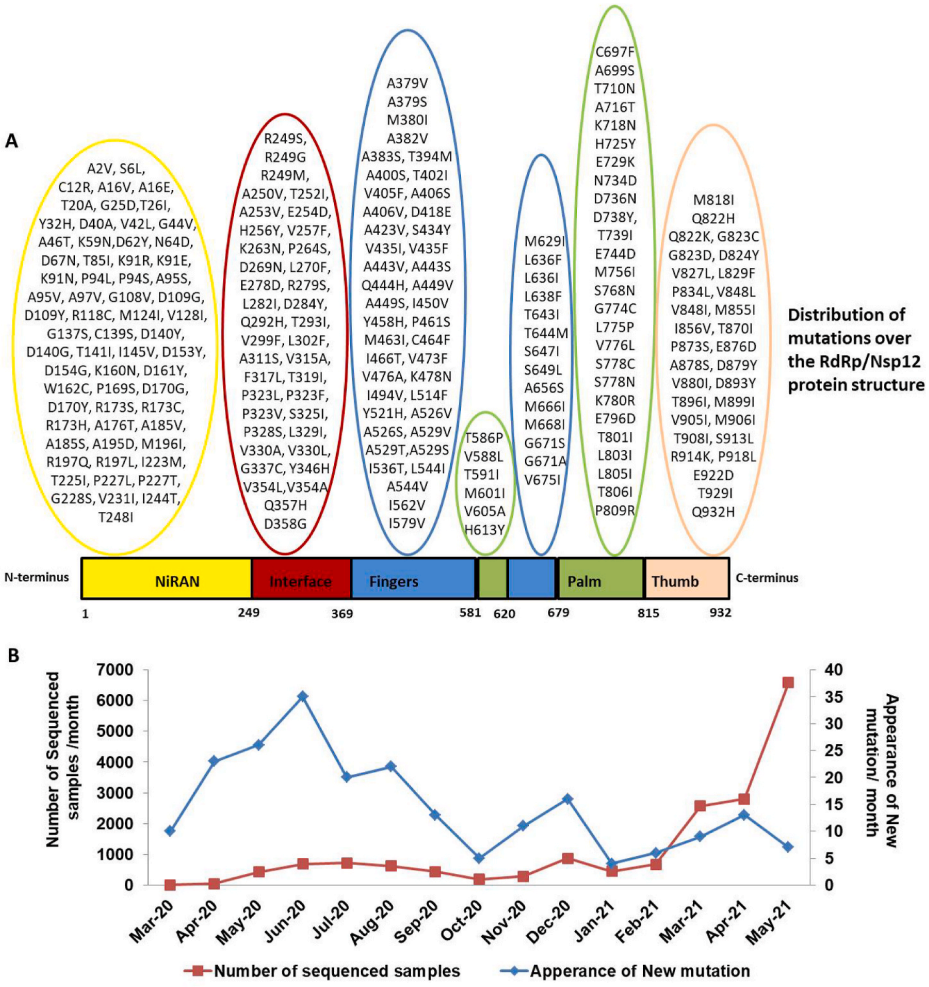

Fig. 1. The details of the mutation identified in RdRp among Indian SARS-CoV-2 isolates. A) Schematic diagram of the domain architecture of RdRp. Each domain of RdRp is represented by a unique color. The interdomain borders are labeled with residue numbers.The mutations present in RdRp among the Indian isolates of SARS-CoV-2 are demonstrated in the schematics. B) The monthly data of 'new sequences' of SARS-CoV-2 and 'appearance of new mutations' were obtained from CoVal webserver. These data provided the time course of the SARS-CoV-2 samples reported from India. Based on the mutational analysis of RdRp by CoVal webserver, we observe that during initial phase COVID19 pandemic, the rate occurrence of new mutations were high but it slowed down as the time progresses. The X-axis shows months/year and Y-axis present on the left side of the graph represents number of SARS-CoV-2 samples reported per month while Y –axis on the right side shows the appearance of new mutation in RdRp per month. (For interpretation of the references to color in this figure legend, the reader is referred to the Web version of this article.)

3.4. RdRp mutants preferentially localises in the B cell epitopes region

Next, we analysed and compared the RdRp mutations that reside in the linear-continuous and discontinuous B cell epitopes. Our data revealed that out of 223 mutants observed in this study, 98 resides in the B cell epitope region of RdRp (Fig. 3A). These 98 mutants correspond to 44% of the total mutants observed among Indian isolates. The details of all 98 mutants that localises in B cell epitope region are shown in Fig. 3B. Altogether, our data strongly suggest that several RdRp mutations localises in the B cell epitope region.

4. Discussion

The coronaviruses belongs to RNA viruses that exhibits high rate of mutations in their genome [21]. As these viruses spread to new locations they keep on acquiring mutations and few of them are naturally selected because of their beneficial effect on the virus. The investigation on the genomic variation acquired by SARS-CoV-2 is indispensable for understanding the epidemiology, pathogenesis; devise preventive measures and treatment strategies against COVID-19. The earlier variation studies on SARS-CoV-2 revealed that RdRp is among the mutational hotspot protein [14]. In the similar directions, this study was conducted with an aim to identify mutations in RdRp from Indian isolates. Our earlier study revealed seven crucial mutations in RdRp of SARS-CoV-2 [22] that can have potential impact on this protein function. The present study identifies and characterises B cell epitope contributed by RdRp and correlate them with the observed mutants. In this study, we analysed 50217 RdRp sequences reported from India till Sept 2021 and identified 223 mutations in RdRp, which indicates that RdRp is one of the mutational hotspot protein of SARS-CoV-2. Furthermore, our data revealed that there are thirty-six high rank linear-continuous B cell epitope as well as twenty-five discontinuous B cell epitopes. Moreover, we also identified that out of 223 mutants identified among Indian isolates, 98 resides (44%) in these B cell epitope region.

We used bioinformatics approach to identify probable epitopes that offer various advantages over conventional approaches. However,

A

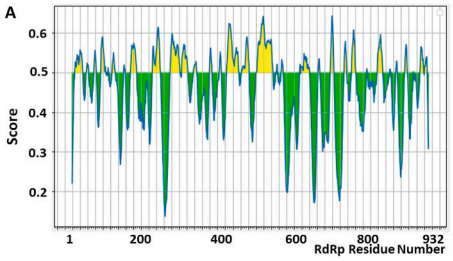

B

Linear- continuous B cell epitopes RdRp

Epitopes	Peptide Start	Peptide End	Peptide Sequence
Peptide 1	8	28	LNRVCGVSAARLTPCGTGTST
Peptide 2	39	44	NDKVAG
Peptide 3	58	64	EKDEDDN
Peptide 4	76	88	TFSNYQHEETIYN
Peptide 5	91	91	K
Peptide 6	95	96	AV
Peptide 7	106	113	IDGDMVPH
Peptide 8	136	139	EGNC
Peptide 9	154	169	DDYFNKKDWYDFVENP
Peptide 10	211	231	DLNGNWYDFGDFIQTTPGSGV
Peptide 11	257	283	VDTDLTKPYIKWDLLKYDFTEERLKLF
Peptide 12	288	303	KYWDQTYHPNCVNCLD
Peptide 13	318	326	STVFPPTSF
Peptide 14	360	366	NLHSSRL
Peptide 15	386	390	NLLLD
Peptide 16	405	436	VAFQTVKPGNFNKDFYDFAVSKGFFK EGSSVE
Peptide 17	444	463	QDGNAAISDYDYYRYNLPTM
Peptide 18	482	525	CYDGGCINANQVIVNNLDKSAGFPF NKWGKARLYYDSMSYEDQD
Peptide 19	533	533	R
Peptide 20	536	537	IP
Peptide 21	547	552	AISAKN
Peptide 22	596	597	GG
Peptide 23	599	621	HNMLKTVYSDVENPHLMGWDYPK
Peptide 24	644	648	TCCSL
Peptide 25	676	685	KPGGTSSGDA
Peptide 26	712	718	GNKIADK
Peptide 27	731	742	LYRNRDVDTDFV
Peptide 28	771	772	AS
Peptide 29	798	812	KCWTETDLTKGPHEF
Peptide 30	832	832	P
Peptide 31	834	834	P
Peptide 32	847	850	IVKT
Peptide 33	871	877	KHPNQEY
Peptide 34	893	893	D
Peptide 35	910	919	DNTSRYWEPE
Peptide 36	922	928	EAMYTPH

C

Discontinuous B cell epitopes of RdRp

Serial Number	RdRp Residue Number	Residue Name	Propensity Score	DiscoTope Score
1	100	ASP	-1.118	-1.335
2	117	GLN	-3.091	-3.656
3	160	LYS	-3.513	-3.224
4	264	PRO	-2.155	-2.137
5	806	THR	-2.879	-3.008
6	819	LEU	-2.672	-3.63
7	820	VAL	-0.879	-3.538
8	821	LYS	3.032	2.453
9	822	GLN	3.022	0.259
10	823	GLY	1.98	0.027
11	824	ASP	2.13	1.885
12	825	ASP	2.327	1.369
13	826	TYR	1.589	0.371
14	873	PRO	0.749	0.088
15	874	ASN	-0.477	-2.262
16	875	GLN	-3.421	-3.258
17	911	ASN	-0.83	-1.08
18	912	THR	-1.647	-2.147
19	913	SER	-2.016	-1.784
20	919	GLU	-1.995	-2.225
21	922	GLU	-1.367	-2.704
22	923	ALA	-0.296	-1.642
23	926	THR	-1.369	-2.592
24	928	HIS	-0.061	-1.204
25	929	THR	-0.89	-2.168

Fig. 2. Prediction of B-cell epitopes of RdRp. A) Linear continuous B-cell epitopes contributed by RdRp, the Y-axis of the graph corresponds to BepiPred score, while the X-axis depicts the RdRp residue positions in the sequence. The data was generated by IEDB webserver using 'Bepipred Linear Epitope Prediction 2.0' method. The chart is divided into two parts, yellow and green. The RdRp residues present in the yellow area have higher probability to be part of the linear continuous B cell epitope. B) The details of the linear continuous B cell epitopes are listed. The sequence of each peptide along with its start and end point in the RdRp polypeptide sequence is also mentioned. C) Prediction of discontinuous B-cell epitopes of RdRp by DiscoTope 2.0 web tool. The position of each predicted epitope is mentioned along with its propensity and DiscoTope score. (For interpretation of the references to color in this figure legend, the reader is referred to the Web version of this article.)

A

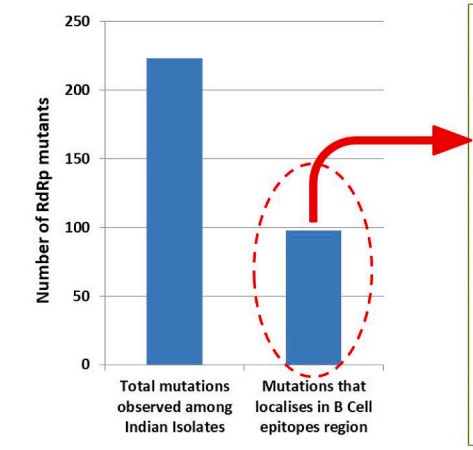

B

Linear- continuous B cell epitopes RdRp/Nsp12

C12R, A16V, A16E, T20A, G25D,T26I, D40A, V42L, G44V, K59N, D62Y, N64D, T85I, K91R, K91E, K91N, A95S, A95V, G108V, D109G, D109Y, G137S, C139S, D154G, K160N, D161Y, W162C, P169S, I223M, T225I, P227L, P227T, G228S, V231I, V257F, K263N, P264S, D269N, L270F, E278D, R279S, L282I, Q292H, T293I, V299F, L302F, T319I, P323L, P323F, P323V, S325I, V405F, A406S, A406V, D418E, A423V, S434Y, V435I, V435F, Q444H, A449V, A449S, I450V, Y458H, P461S, M463I, I494V, L514F, Y521H, T644M, S647I, A716T, K718N, N734D, D736N, D738Y, T739I, T801I, L803I, L805I, T806I, P809R, P834L, V848L, V848I, P873S, E876D, D893Y, S913L, R914K, P918L, E922D

Discontinuous B cell epitopes of RdRp/ NSP12

K160N, P264S, T806I, Q822H, Q822K, G823C, G823D, D824Y, P873S, S913L, E922D, T929I

Fig. 3. Correlation of RdRp mutants and B cell epitopes. A) The graph shows the distribution of RdRp mutants observed among Indian SARS-CoV-2 isolates. Out of 223, 98 mutants localises in B cell epitope region of RdRp. B) Detail of the RdRp mutants that localises in B cell epitope region.

despite advantages of immunoinformatics, there are certain limitations. Such as the final selection of epitopes from the probable epitopes identified using bioinformatics is still a challenging task. The RdRp epitopes revealed in this study requires validation using in vivo experiments, which is slow and herculean task. Furthermore, the algorithms used for predicting epitopes are liable to alter if the criteria are changed during the tool selection. Therefore, the algorithms are constantly improved to get better output and more reliable data [7,8]. The variations in RdRp or any other protein of SARS-CoV-2 will possibly tell us how the virus is evolving. Earlier studies with RNA viruses have also shown that these viruses keep on mutating to better adapt and survive in the host [23]. Here, in this study, we have reported RdRp mutations, its correlation with B cell epitopes. However, it warrants future studies to understand the possible effect of these mutations on virus infectivity and life cycle.

Acknowledgements

We would like to acknowledge Patna University, Patna, Bihar (India) for providing infrastructural support for this study. This work has been partly funded by (Science and Engineering Board, Department of Science and Technology, Government of India) a project awarded to GKA

(Project number: SRG/2020/000808).

References

[1] Wu F, Zhao S, Yu B, Chen YM, Wang W, Song ZG, et al. A new coronavirus associated with human respiratory disease in China. Nature 2020. https://doi.org/10.1038/s41586-020-2008-3.

[2] Chan JFW, Kok KH, Zhu Z, Chu H, To KKW, Yuan S, et al. Genomic characterization of the 2019 novel human-pathogenic coronavirus isolated from a patient with atypical pneumonia after visiting Wuhan. Emerg Microb Infect 2020. https://doi.org/10.1080/22221751.2020.1719902.

[3] Peng Q, Peng R, Yuan B, Zhao J, Wang M, Wang X, et al. Structural and biochemical characterization of nsp12-nsp7-nsp8 core polymerase complex from SARS-CoV-2. Cell Rep 2020. https://doi.org/10.1016/j.celrep.2020.107774.

[4] Te Velthuis AJW, Van Den Worm SHE, Snijder EJ. The SARS-coronavirus nsp7+nsp8 complex is a unique multimeric RNA polymerase capable of both de novo initiation and primer extension. Nucleic Acids Res 2012. https://doi.org/10.1093/nar/gkr893.

[5] Yin W, Mao C, Luan X, Shen D-D, Shen Q, Su H, et al. Structural basis for inhibition of the RNA-dependent RNA polymerase from SARS-CoV-2 by remdesivir. Science 2020. https://doi.org/10.1126/science.abc1560. 80-.

[6] Mcdonald SM. RNA synthetic mechanisms employed by diverse families of RNA viruses. Wiley Interdiscip Rev RNA; 2013. https://doi.org/10.1002/wrna.1164.

[7] Greenbaum JA, Andersen PH, Blythe M, Bui HH, Cachau RE, Crowe J, et al. Towards a consensus on datasets and evaluation metrics for developing B-cell epitope prediction tools. J Mol Recogn 2007. https://doi.org/10.1002/jmr.815.

[8] Soria-Guerra RE, Nieto-Gomez R, Govea-Alonso DO, Rosales-Mendoza S. An overview of bioinformatics tools for epitope prediction: implications on vaccine development. J Biomed Inf 2015. https://doi.org/10.1016/j.jbi.2014.11.003.

[9] Azkur AK, Akdis M, Azkur D, Sokolowska M, van de Veen W, Brüggen MC, et al. Immune response to SARS-CoV-2 and mechanisms of immunopathological changes in COVID-19. Allergy Eur J Allergy Clin Immunol 2020. https://doi.org/10.1111/all.14364.

[10] Yashvardhini N, Kumar A, Jha DK. Immunoinformatics identification of B-and T-cell epitopes in the RNA-dependent RNA polymerase of SARS-CoV-2. Can J Infect Dis Med Microbiol 2021. https://doi.org/10.1155/2021/6627141.

[11] Aftab SO, Ghouri MZ, Masood MU, Haider Z, Khan Z, Ahmad A, et al. Analysis of SARS-CoV-2 RNA-dependent RNA polymerase as a potential therapeutic drug target using a computational approach. J Transl Med 2020. https://doi.org/10.1186/s12967-020-02439-0.

[12] Wang W, Zhou Z, Xiao X, Tian Z, Dong X, Wang C, et al. SARS-CoV-2 nsp12 attenuates type I interferon production by inhibiting IRF3 nuclear translocation. Cell Mol Immunol 2021. https://doi.org/10.1038/s41423-020-00619-y.

[13] Wang Y, Anirudhan V, Du R, Cui Q, Rong L. RNA-dependent RNA polymerase of SARS-CoV-2 as a therapeutic target. J Med Virol 2021. https://doi.org/10.1002/jmv.26264.

[14] Pachetti M, Marini B, Benedetti F, Giudici F, Mauro E, Storici P, et al. Emerging SARS-CoV-2 mutation hot spots include a novel RNA-dependent-RNA polymerase variant. J Transl Med 2020. https://doi.org/10.1186/s12967-020-02344-6.

[15] Madeira F, Park YM, Lee J, Buso N, Gur T, Madhusoodanan N, et al. The EMBL-EBI search and sequence analysis tools APIs in 2019. Nucleic Acids Res 2019. https://doi.org/10.1093/nar/gkz268.

[16] Azad GK. The molecular assessment of SARS-CoV-2 Nucleocapsid Phosphoprotein variants among Indian isolates. Heliyon 2021;7. https://doi.org/10.1016/j.heliyon.2021.e06167.

[17] Vita R, Mahajan S, Overton JA, Dhanda SK, Martini S, Cantrell JR, et al. The immune epitope database (IEDB): 2018 update. Nucleic Acids Res 2019. https://doi.org/10.1093/nar/gky1006.

[18] Rodrigues CHM, Pires DEV, Ascher DB. DynaMut: predicting the impact of mutations on protein conformation, flexibility and stability. Nucleic Acids Res 2018. https://doi.org/10.1093/nar/gky300.

[19] Azad GK. Identification and molecular characterization of mutations in nucleocapsid phosphoprotein of SARS-CoV-2. PeerJ 2021. https://doi.org/10.7717/peerj.10666.

[20] Kringelum JV, Lundegaard C, Lund O, Nielsen M. Reliable B cell epitope predictions: impacts of method development and improved benchmarking. PLoS Comput Biol 2012. https://doi.org/10.1371/journal.pcbi.1002829.

[21] Benvenuto D, Giovanetti M, Ciccozzi A, Spoto S, Angeletti S, Ciccozzi M. The 2019-new coronavirus epidemic: evidence for virus evolution. J Med Virol 2020. https://doi.org/10.1002/jmv.25688.

[22] Chand GB, Banerjee A, Azad GK. Identification of novel mutations in RNA-dependent RNA polymerases of SARS-CoV-2 and their implications on its protein structure. PeerJ 2020;8:e9492. https://doi.org/10.7717/peerj.9492.

[23] Sanjuán R, Domingo-Calap P. Mechanisms of viral mutation. Cell Mol Life Sci 2016. https://doi.org/10.1007/s00018-016-2299-6.